Modeling of four-terminal solar photovoltaic systems for field application

Harikrushna Vahanka, Zeel Purohit, and Brijesh Tripathi

Citation: AIP Conference Proceedings **1961**, 030035 (2018); doi: 10.1063/1.5035237
View online: https://doi.org/10.1063/1.5035237
View Table of Contents: http://aip.scitation.org/toc/apc/1961/1
Published by the American Institute of Physics

Modeling of Four-terminal Solar Photovoltaic Systems For Field Application

Harikrushna Vahanka[1], Zeel Purohit[1], Brijesh Tripathi[1,a)]

[1]*Department of Science, School of Technology, Pandit Deendayal Petroleum University, Raisan, Gandhinagar – 382007 India.*

[a)]*Corresponding author:* brijesh.tripathi@sse.pdpu.ac.in

Abstract. In this article a theoretical framework for mechanically stacked four-terminal solar photovoltaic (FTSPV) system has been proposed. In a mechanical stack arrangement, a semitransparent CdTe panel has been used as a top sub-module, whereas a μc-Si solar panel has been used as bottom sub-module. Theoretical modeling has been done to analyze the physical processes in the system and to estimate reliable prediction of the performance. To incorporate the effect of material, the band gap and the absorption coefficient data for CdTe and μc-Si panels have been considered. The electrical performance of the top and bottom panels operated in a mechanical stack has been obtained experimentally for various inter-panel separations in the range of 0-3 cm. Maximum output power density has been obtained for a separation of 0.75 cm. The mean value of output power density from CdTe (top panel) has been calculated as 32.3 Wm^{-2} and the mean value of output power density from μc-Si, the bottom panel of four-terminal photovoltaic system has been calculated as ~3.5 Wm^{-2}. Results reported in this study reveal the potential of mechanically stacked four-terminal tandem solar photovoltaic system towards an energy-efficient configuration.

INTRODUCTION

Solar energy is the major fraction of renewable energy with the energy radiated by Sun at a rate of 4.3×10^{20} J/hr [1]. Solar photovoltaic (PV) panels are used for direct conversion of solar energy into electrical energy. The crystalline silicon (c-Si) solar PV technology has been dominating the solar energy market for several decades, with a current market share of ~90% [2]. During last decade there has been only marginal increase in the efficiency of the crystalline silicon solar PV technology. Energy conversion efficiency as high as 25.6% has been obtained using amorphous silicon (a-Si)/c-Si heterojunction technology [3]. Recently an efficiency of 26.3% has been obtained on 180 cm^2 crystalline silicon solar cell [4], which is close to the theoretical maximum efficiency of 29.4% [5]. In order to utilize solar spectrum to a greater extent and obtain high efficiency at a lower cost, tandem approaches have been proposed by many researchers [6-12]. In tandem approach, which combines small band-gap and large band-gap solar energy absorber materials to utilize the solar spectrum up to greater extent, the large bandgap solar cell is generally placed as top subcell, and small bandgap solar cell is generally placed as bottom subcell. There are two major approaches to fabricating Si based tandem solar cells: epitaxial growth [13-18] and mechanical stacking [19-27]. Compared to the common 2-terminal tandem structure in monolithic series connection, the 4-terminal tandem structure has several advantages: no need of current or lattice matching, simple mechanical stacking, and more freedom for choosing the top and bottom cells. Most of the available literature reports the data on the development of tandem structure at the solar cell level, whereas there are few reports on the mechanically stacked 4-terminal solar PV module performance. This article aims to develop theoretical framework for analyzing the outdoor electrical performance of the mechanically stacked 4-terminal solar PV module technology. For realistic calculations, an example of currently commercialized thin-film technology based modules made of cadmium telluride (CdTe) and micro-crystalline silicon (μc-Si) have been chosen in this study. The reported theoretical model can also be used for electrical performance assessment of the other solar PV technologies.

THEORETICAL BACKGROUND

The P-N junction diode based equations have been used for electrical performance evaluation of mechanically stacked solar PV modules. The theoretical model uses the charge carrier transport properties of each semiconductor material and its light absorption profile. It is assumed that the P-N junction behaves according to the ideal single diode model where each absorbed photon creates one electron-hole pair and the generated charge carriers are prone to recombination losses. It is important to note that this theoretical model includes optical losses due to reflection at the surface and the interface of the solar PV modules.

International Conference on Nanomaterials for Energy Conversion and Storage Applications
AIP Conf. Proc. 1961, 030035-1–030035-7; https://doi.org/10.1063/1.5035237
Published by AIP Publishing. 978-0-7354-1666-6/$30.00

The light generated current density, J_{PH} (mAcm^{-2}), in a thin-film PV module can be determined using the AM1.5 Direct Solar Spectrum from the ASTM G-173-03 reference standard [28]. The photon flux ($\phi(\lambda)$, #photons m^{-2}s^{-1}) incident on a solar panel has been calculated using Eq. (1), where $I_0$is the power (W m^{-2} nm^{-1}) of the AM1.5 Direct Solar spectrum at wavelength λ (nm):

$$\phi(\lambda) = \frac{I_0}{h \cdot c/\lambda} \Delta\lambda \tag{1}$$

The semiconductor material absorption coefficient (α) data with respect to the wavelength (λ) and the thickness (x) in the solar PV module have been used to calculate J_{PH}. The absorption coefficient data as shown in Fig. 3 have been taken from the literature [29, 30].The light generated current density, J_{PH}, is related to the incident number of photons absorbed across the entire thickness of the absorbing layer using Eq. (2) [31]:

$$J_{PH} = \int_{\lambda=400\,nm}^{\lambda=1100\,nm} q \cdot \phi(\lambda) \cdot \left(1 - R(\lambda)\right) \cdot \left(1 - e^{-\alpha(\lambda) \cdot x}\right) \cdot \Delta\lambda \tag{2}$$

where, q represents the electron charge and R(λ) represents the reflected part of incident spectrum from the surface or interface of the mechanical stack. For the case of mechanically stacked 4-terminal arrangement of solar PV modules based on CdTe and μc-Si technology, it is considered that the part of incident spectrum on the second module has been adjusted for absorption in the first module through the Eq. (3) [31]:

$$I_1(\lambda) = I_0(\lambda) \cdot e^{-\alpha(\lambda) \cdot d_{\mu c-Si}} \tag{3}$$

where, I_1 represents the part of incident spectral power on second module of mechanical stack, I_0 represents the incident spectral power on first module. The value of spectral power can be used in Eq. (1) to find corresponding photon flux and then the light generated current density can be calculated from Eq. (2). The spectral power distribution with respect to the wavelength and in comparison to the absorption coefficients of CdTe and μc-Si is shown in Fig. 1.

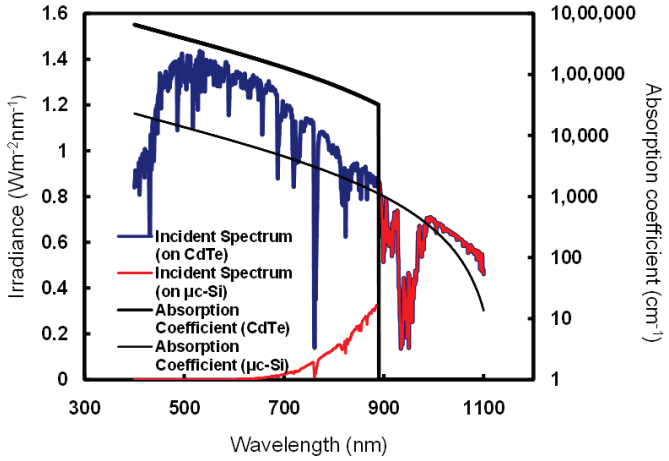

Figure 1: The spectral power distribution with respect to the wavelength and in comparison to absorption coefficients of CdTe and μc-Si.

The Shockley single-diode equation for electrically homogeneous semiconductor absorber material can be written as [32, 33]:

$$J = J_{PH} - J_0 \cdot \left\{\exp\left(\frac{q \cdot (V + J \cdot R_S)}{n \cdot k_B \cdot T}\right) - 1\right\} - \frac{(V + J \cdot R_S)}{R_{SH}} \tag{4}$$

where, J represents the current density measured across the terminal electrodes, V represents the voltage measured across the terminal electrodes, J_{PH} represents the photo-generated current density, J_0 represents the reverse saturation current density, q represents the electron's charge, R_S represents the series resistance, R_{SH} represents the shunt resistance, k_B represents the Boltzmann constant, T represents the absolute temperature, and n represents the diode-ideality factor.The reverse saturation current density, J_0, has been calculated as the sum of the contributions of the n- and p-type materials assuming uniform doping in each one of them and expressed as given below [34]:

$$J_0 = q \cdot n_i^2 \cdot \left(\frac{D_e}{N_A \cdot L_e} + \frac{D_h}{N_D \cdot L_h}\right) \quad (5)$$

where, n_i represents the intrinsic carrier concentration, D_e represents the diffusion coefficient of electrons, D_h represents the diffusion coefficient of holes, N_A represents the acceptor concentration in the n-type material, N_D represents the donor concentration in the p-type material, L_e and L_h represent the diffusion lengths of electrons and holes respectively.The open-circuit voltage (V_{OC}) and fill factor (FF) of the solar panels under illumination are expressed as below for the ideal conditions, i.e. $R_S \rightarrow 0$ and $R_{SH} \rightarrow \infty$:

$$V_{OC} = \frac{k_B \cdot T}{q} ln\left(\frac{J_{PH}}{J_0} + 1\right) \quad (6)$$

$$FF = 1 - \frac{k_B \cdot T}{q \cdot V_{OC}} \ln \frac{q \cdot V_{OC}}{k_B \cdot T} - \frac{J_{PH} \cdot R_S}{V_{OC}} \quad (7)$$

The maximum power output of the solar panel is related to short-circuit current, J_{SC} and FF as per following expression:

$$P_m = FF \cdot V_{OC} \cdot J_{SC} \quad (8)$$

Individual solar panels in a mechanical stack arrangement are generally connected in parallel so as to allow separate load control of each panel [31].

EXPERIMENTAL DETAILS

Experiments have been performed at Samroli village, Navsari, India with longitude of 73.04074° and latitude of 20.77575°. The values of irradiance and ambient temperature have been recorded as 500±50 Wm^{-2} and 31 °C respectively. Semi-transparent CdTe and µc-Si solar panels have been purchased from the market and arranged in a manner shown in Fig. 2. The performance parameters of the semi-transparent CdTe and µc-Si panels under standard test conditions (STC, 25 °C, 1000 Wm^{-2}) are listed in Table 1.

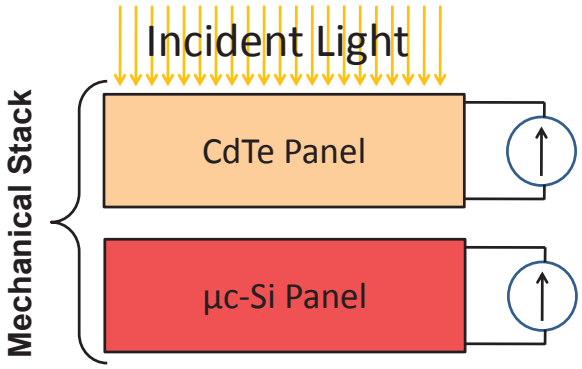

Figure 2: Schematic representation of mechanical stack arrangement of four-terminal photovoltaic system to extract experimental data.

Table 1: Performance parameters of the semitransparent CdTe and µc-Si panels under standard test conditions.

Parameter	CdTe Panel	µc-Si Panel
Area (m^2)	0.7200	0.7905
Transmission (%)	50	40
I_{SC} (A)	0.62	0.75
V_{OC} (V)	116	79
FF (%)	55	59
P_{MAX} (W)	40	35

RESULTS AND DISCUSSION

The output power density of cadmium telluride (CdTe) and microcrystalline silicon (μc-Si) panels have been measured in four-terminal arrangement as shown in Fig. 3. Small variation in the output of the top panel has been recorded due to the variation in the intensity of light due to the presence of very thin layer of clouds during the measurements. In order to calculate overall effect, the mean value of output power density has been considered and marked in Fig. 3. The mean value of output power density from CdTe (top panel) has been calculated as 32.3 Wm^{-2} and the mean value of output power density from μc-Si, the bottom panel of four-terminal photovoltaic system has been calculated as ~3.5 Wm^{-2}. The mean value of total output power density of the four-terminal photovoltaic system has been calculated as 35.8 Wm^{-2}. The measurements have been performed for various values of inter-panel separation varied in the range of 0-3 cm. It is clearly observed from these measurements that the bottom panel performs best for an inter-panel separation of 0.75 cm, which can be confirmed from further analysis. In order to further understand the effect of inter-panel separation, the performance parameters (J_{SC}, V_{OC}, FF and P_{MAX}) have been plotted with respect to the separation. The variation of short-circuit current density from μc-Si panel placed below CdTe panel with respect to the space between CdTe and μc-Si panels is shown in Fig. 3. The percentage deviation in the measurements has been found to be within ±10% of the mean value.

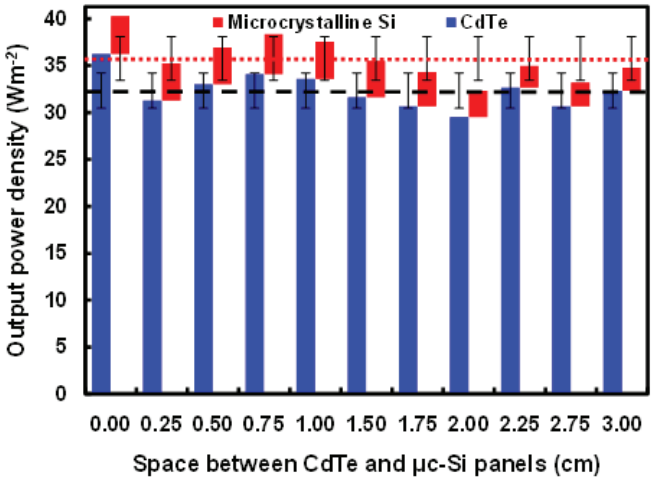

Figure 3: Output power density of cadmium telluride (CdTe) and microcrystalline silicon (μc-Si) panels in four-terminal arrangement. Error bars represent standard deviation from mean value. Dashed line represent mean value (32.3 Wm^{-2}) of power output from CdTe (top) and dotted line represent mean value (35.8 Wm^{-2}) of power output from four-terminal photovoltaic system with μc-Si as a bottom panel.

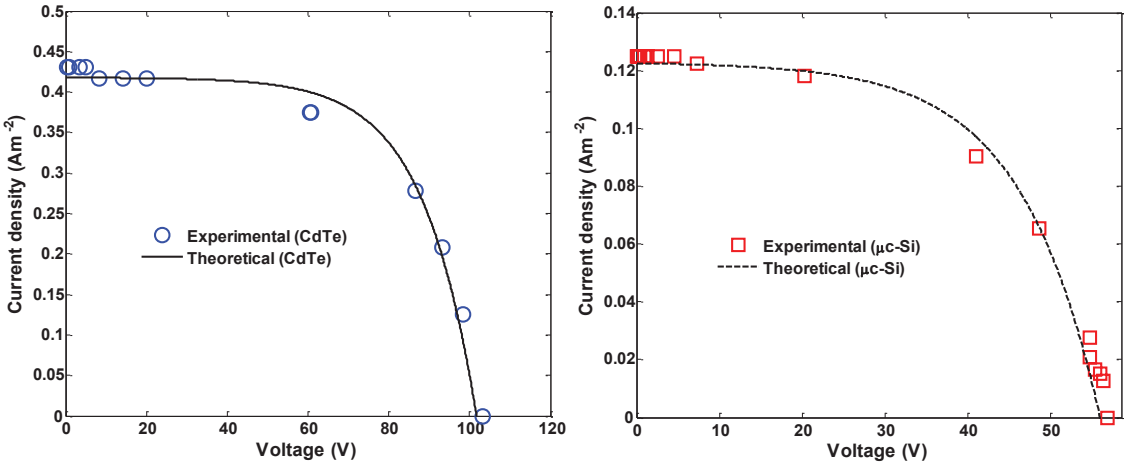

Figure 4: (a) Experimental and theoretical J-V curve of CdTe panel and (b) Experimental and theoretical J-V curve of μc-Si panel.

Figures 4(a) and 4(b) showcombined experimental and theoretical J-V curves of CdTe and µc-Si panels respectively. The theoretical curves have been generated by fitting experimental data using Eq. (4). In order to fit experimental data of CdTe panel, J_{PH}, J_0, R_S, R_{SH}, and n havebeen taken as 0.86 Am^{-2}, 1.1×10^{-4} Am^{-2},0.015 Ω, 3000 Ω, and 4.1 respectively. The J-V curve has been generated for an illumination intensity of 48 Wm^{-2}. Further, in order to fit experimental data of µc-Si panel, J_{PH}, J_0, R_S, R_{SH}, and n havebeen taken as 1.04 Am^{-2}, 2.4×10^{-4} Am^{-2}, 0.015 Ω, 1000 Ω, and 3.6 respectively. The J-V curve has been generated for an illumination intensity of 117Wm^{-2}. Table 2 lists out various parameters of Eq. (5) to calculate the values of J_0 for both the panels.

Table 2: Various parameters to calculate reverse saturation current density J_0

Parameter	CdTe Panel	µc-Si Panel
D_e (cm^2/s)	27 [34]	3.75 [37]
D_h(cm^2/s)	2.6 [34]	12.5 [37]
N_A (m^{-3})	1.8×10^{20}[35]	1×10^{20} [38]
N_D(m^{-3})	2.24×10^{20}[35]	1×10^{20} [38]
n_i(m^{-3})	7×10^{15} [36]	8.3×10^{15} [39]
L_h(µm)	1 [34]	0.6 [37]
L_e(µm)	1 [34]	0.6 [37]
J_0 (mA^{-2})	1.1×10^{-4}	2.4×10^{-4}

In Fig. 5 (a) and 5(b) the performance parameternamely short-circuit density and open-circuit voltage has been plotted as a function of separation space between the panels. In Fig. 4(a), the short-circuit current density remains constant for a separation space of up to 1.5 cm and starts decreasing beyond this separation. This trend is attributed to the reduction in the light intensity, while light passes through the top panel. After passing through the top panel, the light diverges and effective intensity per unit area decreases, which results in the reduction of short-circuit current density of the bottom panel. The observed behavior is in accordance with the known linear dependence of the J_{SC} on the intensity of illumination [33]. The open-circuit voltage is plotted with respect to the space between the CdTe and µc-Si panels in Fig. 5(b). V_{OC} is found to decrease slowly with increasing separation beyond 1.5 cm, which may be attributed to the logarithmic dependence of V_{OC} on the intensity of illumination. The decrease in the intensity of illumination has already been confirmed from the J_{SC} data. Logarithmic dependence of V_{OC} on illumination intensity has been well documented [34]. A decrease beyond the logarithmic limits has not been observed in the V_{OC}, which confirms that there is no additional mechanism in this decrease of V_{OC}.

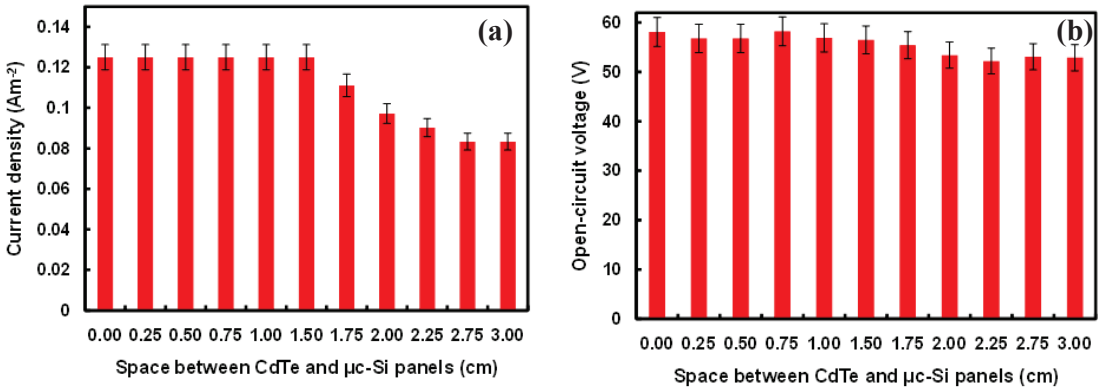

Figure 5: (a) Variation of short-circuit current density from µc-Si panel placed below CdTe panel with respect to the space between CdTe and µc-Si panels, (b)Variation of open-circuit voltage of µc-Si panel placed below CdTe panel with respect to the space between CdTe and µc-Si panels. Error bars represent a deviation of ±5%.

The variation of fill factor and power output density has been plotted with respect to the space between CdTe and µc-Si panels in Fig. 5. There is no significant variation in the fill factor with respect to the space between CdTe and µc-Si panels as shown in Fig. 5(a). This observation confirms that the fill factor of the thin film µc-Si based panel is insensitive to the small variation in the intensity of illumination. Further, the maximum output power density of the µc-Si panel placed below the CdTe panel has been plotted with respect to the space between these panels and shown in Fig. 5(b).

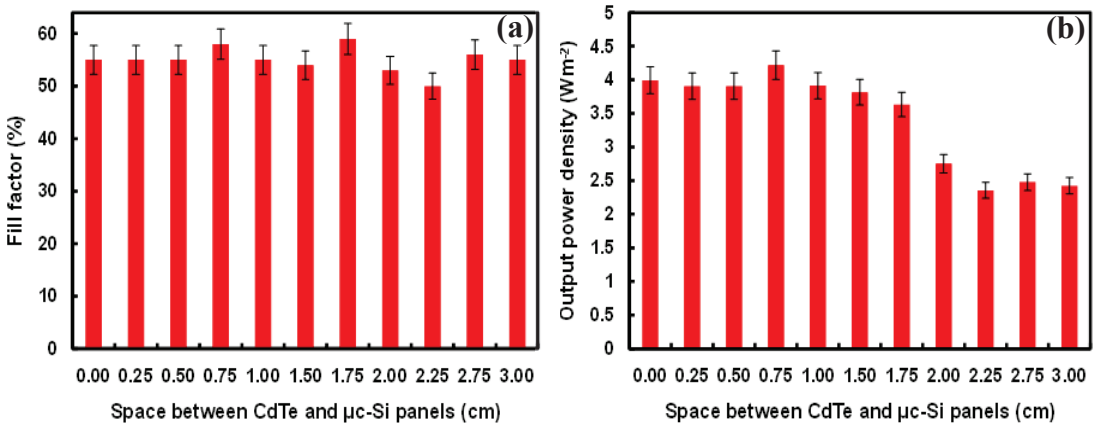

Figure 6: (a) Variation of fill factor of µc-Si panel placed below CdTe panel with respect to the space between CdTe and µc-Si panels, (b) Variation of output power density of µc-Si panel placed below CdTe panel with respect to the space between CdTe and µc-Si panels. Error bars represent a deviation of ±5%.

Maximum output power density is governed by the Eq. (8) and depends on the J_{SC}, V_{OC} and FF. A combined effect of all the three parameters has been observed on the power density, but it is dominated by the trend of J_{SC}, which can be seen by comparing Fig. 6 (b) with Fig. 5 (a). A decreasing trend of power density beyond a separation of 1.5 cm confirms the effect linear dependence of J_{SC} on intensity of illumination. Maximum output power density has been obtained for a separation of 0.75 cm.

CONCLUSIONS

A theoretical framework for mechanically stacked four-terminal solar photovoltaic (FTSPV) system has been established. Theoretical modeling has been done to analyze the physical processes in the system and to estimate reliable predictions of the performance. The electrical performance of the top and bottom panels operated in a mechanical stack has been obtained experimentally for various inter-panel separations in the range of 0-3 cm. Maximum output power density has been obtained for a separation of 0.75 cm. The mean value of output power density from CdTe (top panel) has been calculated as 32.3 Wm^{-2} and the mean value of output power density from µc-Si, the bottom panel of four-terminal photovoltaic system has been calculated as ~3.5 Wm^{-2}. Results reported in this study reveal the potential of mechanically stacked four-terminal tandem solar photovoltaic system towards an energy-efficient configuration.

REFERENCES

1. N. S. Lewis, "Basic research needs for solar energy utilization", in Proceedings of the Basic Energy Sciences Workshop on Solar Energy Utilization Chair, California Institute of Technology, 2005.
2. M. Wang, X. Gu, P. Ma, W. Zhang, D. Yu, P. Chang, X. Chen and D. Li, Mat. Res. Bull. **91,** 208-213 (2017).
3. K. Masuko, M. Shigematsu, T. Hashiguchi, D. Fujishima, M. Kai and N. Yoshimura, PHOT, IEEE J. Photovolt. **4**, 1433-1435 (2014).
4. Kaneka corporation. http://www.kaneka.co.jp/en/images/topics/1473811995/1473811995_101.pdf (accessed on 19-09-2017)
5. A. Richter, M. Hermle and S. W. Glunz, Phot IEEE J. Photovolt. **3**, 1184-1191 (2013).
6. G. Sun, F. Chang and R. A. Soref, Opt.Express**18**, 3746-3753 (2010).
7. X. Sheng, C.A. Bower, S. Bonafede, J.W. Wilson, B. Fisher, M. Meitl, H. Yuen, S. Wang, L. Shen, A.R. Banks, C.J. Corcoran, R.G. Nuzzo, S. Burroughs and J.A. Rogers, Nat. Mater **13**, 593–598 (2014).
8. D. Bailie, M. G. Christoforo, J. P. Mailoa, A. R. Bowring, E. L. Unger, W. H. Nguyen, J. Burschka, N. Pellet, J. Z. Lee, M. Grätzel, R. Noufi,. T. Buonassisi, A. Salleo and M. D. McGehee, Energy Environ. Sci. **8**, 956 (2015).
9. R. King, D. Law, K. Edmondson, C. Fetzer, G. Kinsey, H. Yoon, R. Sherif and N. Karam, Appl. Phys. Lett. **90**, 183516 (2007).

10. P. Löper, S. J. Moon, S. Martín de Nicolas, B. Niesen, M. Ledinsky, S. Nicolay, J. Bailat, J.-H.Yum, S. De Wolf and C. Ballif, Organic–inorganic halide perovskite/crystalline silicon four-terminal tandem solar cells, Phys. Chem. Chem. Phys. **17**, 1619 (2015).
11. J. F. Geisz, D. J. Friedman, J. S. Ward, A. Duda, W. J. Olavarria, T. E. Moriarty, J. T. Kiehl, M. J. Romero, A. G. Norman and K. M. Jones, Appl. Phys. Lett. **93**, 123505 (2008).
12. W. Guter, J. Schöne, S. Philipps, M. Steiner, G. Siefer, A. Wekkeli, E. Welser, E. Oliva, A. Bett and F. Dimroth, Appl. Phys. Lett. **94**, 223504 (2009).
13. F. Dimroth, M. Grave, P. Beutel, U. Fiedeler, C. Karcher, T. Tibbits, E. Oliva, G. Siefer, M. Schachtner, A. Wekkeli, A. Bett, R. Krause, M. Piccin, N. Blanc, C. Drazek, E. Guiot, B. Ghyselen, T. Salvetat, A. Tauzin, T. Signamarcheix, A. Dobrich, T. Hannappel and K. Schwarzburg, Prog. Photovolt. Res. Appl. **22**, 277-282 (2014).
14. M. Green, K. Emery, Y. Hishikawa, W. Warta and E. Dunlop, Prog. Photovolt. Res. Appl. **24**, 905-913(2016).
15. Y. Itoh, T. Nishioka, A. Yamamoto and M. Yamaguchi, Appl. Phys. Lett. **49**, 1614-1616 (1986).
16. S. Ringel, J. Carlin, C. Andre, M. Hudait, M. Gonzalez, D. Wilt, E. Clark, P. Jenkins, D. Scheiman, A. Allerman, E. Fitzgerald and C. Leitz, Prog. Photovolt. Res. Appl. **10**, 417-426 (2002).
17. J. F. Geisz, J. M. Olson, M. J. Romero, C. S. Jiang and A. G. Norman, "Lattice-mismatched GaAsP Solar Cells Grown on Silicon by OMVPE", 2006 IEEE 4th World Conference on Photovoltaic Energy Conference, 2006.
18. Y. B. Bolkhovityanov and O. P. Pchelyakov, Physics-Uspekhi 51, 437–456 (2008).
19. S. Hassan, Four-Terminal Mechanically Stacked GaAs/Si Tandem Solar Cells, University of Michigan, arXiv:1505.06711 (2015).
20. R. Gehlhaar, D. Cheynsa, L. V. Willigenburga, A. Hadipoura, J. Gilotb, R. Radbehc and T. Aernoutsa, Proc. of SPIE 8830, 1-13(2013).
21. J. M. Gee and G. F. Virshup, "A 31%-efficient GaAs/silicon mechanically stacked, multijunction concentrator solar cell," in Conference Record of the20th. IEEE Photovoltaic Specialists Conference (PVSC), Las Vegas, NV, USA, 754-758(1988).
22. Y. Yazawa, K. Tamura, S. Watahiki, T. Kitatani, H. Ohtsuka and T. Warabisako, Three-junction solar cells comprised of a thin-film GaInP/GaAs tandem cell mechanically stacked on a Si cell, Conference Record of the Twenty Sixth IEEE Photovoltaic Specialists Conference, 899-902 (1997).
23. J.M. Zahler, A. F. Morral, C. Ahn, H. Atwater, M. Wanlass, C. Chu and P. Iles, Wafer bonding and layer transfer processes for 4-junction high efficiency solar cells, Conference Record of the Twenty-Ninth IEEE Photovoltaic Specialists Conference, 1039-1042(2002).
24. H. Taguchi, T. Soga and T. Jimbo, Jpn. J. Appl. Phys **42**, L1419–L1421 (2003).
25. Vishnuvardhanan, Vijayakumar, Journal of Solar Energy Engineering **136**, 1-7 (2014).
26. M. Jaysankar, W. Qiu, M. V. Eerden, T. Aernouts, R. Gehlhaar, M. Debucquoy, U. W. Paetzold and J. Poortmans, Adv. Energy Mater. **7**, 1-8 (2017).
27. K.H Lee, K. Nakamura, T. Kamioka, N. Kojima, H. Lee, L. Wang, K. Araki, Y. Ohshita, A. Ogura, M. Yamaguchi, "Fabrication and Performance Analysis of a Mechanical Stack InGaP/GaAs//Si Solar Cell", 43rd IEEE PVSC, Portland, USA, 2016.
28. NREL, "ASTM (G-173-03)", http://rredc.nrel.gov/solar/spectra/am1.5/ (accessed on 12-08-2017).
29. W. W. Yu, L. Qu, W. Guo and X. Peng, Chem. Mater. 15, 2854-2860 (2003).
30. F. Demichelis, E. M. Mezzetti, A. Tagliaferro and E. Tresso, J. Appl. Phys **59**, 611 (1986).
31. I. Mathews, D. O'Mahony, B.Corbett and Alan P. Morrison, Opt. Express **20**, A754 (2012).
32. J. Ma, T. Ting, K. Man, N. Zhang, S. Guan and P. Wong, Journal of Applied Mathematics **67**, 1-8 (2013).
33. P. Yadav, B. Tripathi, M. Lokhande, and M. Kumar, J. Renew. Sustain. Energy **5**, 013113 (2013).
34. C. S. Solanki, Solar Photovoltaics Fundamentals, Technologies and Applications, 2nd ed. New Delhi, India: PHI Learning Private Limited, 2011.
35. M. Hadrich, H. Metzner, U. Reislohner and C. Kraft, Sol. Energy Mater Sol. Cells **95**, 887-893 (2011).
36. C. H. Su, J. Appl. Phys **103**, 084903 (2008).
37. S. Isoda, J Environ Sci **25**, S172–S179 (2013) .
38. M. Sharma, S. Kumar, N. Dwivedi, S.Juneja, A.K. Gupta, S. Sudhakar and K. Patel, Solar Energy **97**, 176-185 (2013).
39. P. P. Altermatt, A. Schenk, F.Geelhaar and G. Heiser, J. Appl. Phys **93**, 1598 (2003).